POLAR RESEARCH, 2018
VOL. 37, 1442982
https://doi.org/10.1080/17518369.2018.1442982

RESEARCH ARTICLE

OPEN ACCESS Check for updates

Radiogenic isotope (Nd, Pb, Sr) signatures of surface and sea ice-transported sediments from the Arctic Ocean under the present interglacial conditions

Jenny Maccali[a], Claude Hillaire-Marcel[a] & Christelle Not [b]

[a]Geotop-UQÀM, Department of Earth and Atmosphere Sciences, Succ. Centre-Ville, Montreal, Québec, Canada; [b]Department of Earth Sciences, The University of Hong Kong, Hong Kong, China

ABSTRACT

Under modern conditions, sediments from the large continental shelves of the Arctic Ocean are mixed by currents, incorporated into sea ice and redistributed over the Arctic Basin through the Beaufort Gyre and Trans-Polar Drift major sea-ice routes. Here, compiling data from the literature and combining them with our own data, we explore how radiogenic isotopes (Sr, Pb and Nd) from Arctic shelf surface sediment can be used to identify inland and coastal sediment sources. Based on discriminant function analyses, the use of two-isotope systematics introduces a large uncertainty (ca. 50%) that prevents unequivocal identifications of regional shelf signatures. However, when using all three isotopic systems, shelf provinces can be distinguished within a ca. 23% uncertainty only, which is mainly due to isotopic overlaps between the Canadian Arctic Archipelago and the Barents–Kara seas areas. Whereas the Canadian Arctic shelf seems mostly influenced by Mackenzie River supplies, as documented by earlier studies, a clear Lena River signature cannot be clearly identified in the Laptev–Kara seas area. The few available data on sediments collected in sea-ice rafts suggest sea ice originating mostly from the Laptev Sea area, along with non-negligible contributions from the East Siberian and Kara seas. At last, whereas a clear radiogenic identity of the Mackenzie River in sediments can be identified in the Beaufort Sea margin, isotopic signatures from major Russian rivers cannot be deciphered in modern Siberian margin sediments because of an intense mixing by sea ice and currents of inland and coastal supplies.

KEYWORDS

Surface shelf sediments; discriminant function analysis; sediment mixing; unequivocal source identification; three-isotope system

ABBREVIATIONS

BS: Barents Sea; CAA: Canadian Arctic Archipelago; CS: Chukchi Sea; ESS: East Siberian Sea; KS: Kara Sea; LS: Laptev Sea

Introduction

A critical feature of the modern Arctic Ocean is the large extent of its shelves that currently represent almost half of its areal extent (Fig. 1). Modern terrigenous sediments accumulate on these shelves, where most of the primary productivity and sea-ice production also take place (Stein 2008; Macdonald & Gobeil 2012). During the last decade, millenial scale, large amplitude changes in Arctic sea-ice dynamics have been documented from deep-sea and shallow sediment core studies based on detailed mineralogical studies of ice-rafted debris (e.g., Phillips & Grantz 2001; Darby 2003; Darby & Bischof 2004; Darby et al. 2011; Darby et al. 2015). More recently, biomarkers, radiogenic isotope compositions and clay minerals from fine sedimentary fractions have also added to our knowledge of Arctic sea-ice history and its linkage with climate (e.g., Wahsner 1999; Knies et al. 2000; Vogt & Knies 2008; Maccali et al. 2012, 2013; Hillaire-Marcel et al. 2013; Navarro-Rodriguez et al. 2013; Fagel et al. 2014). For example, radiogenic isotope (Pb, Sr, Nd) records in deep-sea cores from the Lomonosov Ridge and Fram Strait areas (Hillaire-Marcel et al. 2013), were used to document changes in detrital sedimentary fluxes and ice-rafted debris, from the last glacial interval to the present. Similarly, radiogenic isotopes (Pb, Nd) from the Mendeleev Ridge were used to identify changes in sediment supplies over glacial/interglacial periods (Fagel et al. 2014). However, the Arctic Ocean is a semi-enclosed basin surrounded by vast continental units of various age and composition (Fig. 1; Harrison et al. 2008) making it difficult to link ice-rafted sediments to specific continental areas based on a limited number of radiogenic tracers, as sources have not yet been unequivocally identified. The use of a bedrock database (Fagel et al. 2014) and mean bedrock age model (Peucker-Ehrenbrink et al. 2010) give useful information on the isotopic signature of material potentially delivered through land drainage. However, if shelf sediments relate to river discharge, coastal erosion seems a significant source of sediments in the Arctic Ocean. For example, coastal erosion is important on the wide and shallow Russian shelves, where it accounts for more than 50% of the supply budget, and up to 100% in the specific case of the CS shelf, where river supply is limited (Rachold et al. 2004). In contrast, the Beaufort shelf receives primarily Mackenzie River supplies as this river delivers as much sediments as all other major Arctic rivers combined (Macdonald et al. 2015 and references therein). Once deposited on shelves, the sediments will then be redistributed via currents, uploading in sea ice (i.e., incorporation of suspended particles during ice formation (e.g., Eicken et al. 2005) and then via sea-ice

CONTACT Jenny Maccali jenny.maccali@gmail.com Geotop-UQÀM, CP 8888, Succ. Centre-Ville, Montreal, H3C 3P8 Québec, Canada.
Supplemental data for this article can be accessed here.

transport. These processes have been documented (e.g., Darby 2003) but their overall importance with respect to the final tracer signatures of the Arctic sediments at large remain open to discussion.

Here, we analysed modern surface sediments from the Arctic margins for their radiogenic isotope signatures, as such sediments might reflect best what is currently uploaded by sea ice and re-circulated within the Arctic Ocean and re-deposited as ice-rafted debris. Radiogenic isotopes in sediments bear the same isotopic composition as the rock source and hence are used as tracers of continental inputs (e.g., Goldstein et al. 1984; Goldstein & Hemming 2003). About 30 new sampling sites were added to the about 80 already reported in recent literature (see Table 1, Supplementary Table S1). We also analysed a few sediment samples from ice rafts. Statistical analyses of the surface sediment database now available provides a means to define isotopic clusters in relation with circum-Arctic shelf areas. However, we show that linkages between sediment isotopic composition and continental sources still remain in part equivocal because of large uncertainty in the statistical results.

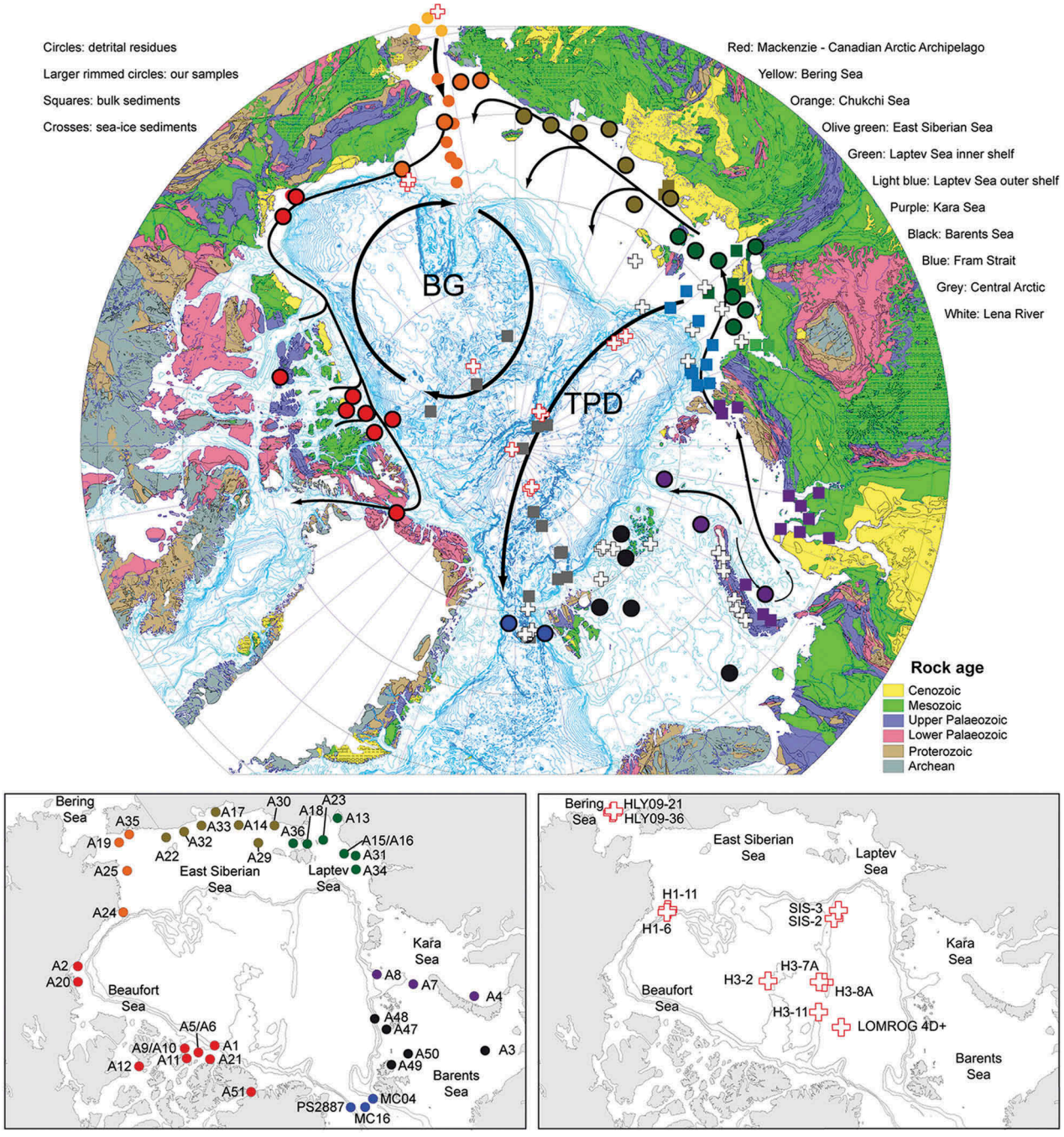

Figure 1. Lithologic map of the Arctic (modified from Harrison et al. 2008) showing shelf-sediment sample locations. The Beaufort Gyre and Trans-Polar Drift are abbreviated as BG and TPD, respectively.

Material and methods

Sediment samples

Surface sediments from shelves and ridges (Fig. 1, Table 1), mostly retrieved from core archives, were sub-sampled in the upper 10 cm of core-tops (with rare exceptions). Surface margin sediments were wet sieved at 100 μm to avoid biases linked to very coarse grains, and leached (see below) in order to analyse the detrital fraction. The time span represented by these samples differs considerably between sites on account of variable sedimentation rates and benthic mixing processes, as well as possible coring artifacts. Nonetheless, all samples may be seen as illustrating late Holocene sedimentation.

Sea-ice samples

A few sediment samples from sea-ice rafts were collected during recent cruises of the German *Polarstern* and US Coast Guard Cutter *Healy* research vessels. Most samples were sieved at 45 μm (Table 2) for bulk x-ray diffraction mineralogy (Darby et al. 2011) except for four samples that were analysed as bulk (i.e., SIS 2–3 and HLY0901–21). However, as the <45 μm grain-size fraction of those three bulk samples represent more than 95% of the total dry weight (Table 2), they can be compared with the <45 μm-sieved sea-ice samples within a small added uncertainty. Samples were chemically untreated prior to their handling in the laboratory. These samples are thought to represent sedimentary material uploaded at places of sea-ice formation (e.g., sea-ice factories; Reimnitz et al. 1994), with possibly some eolian supplies (Maccali et al. 2013), although these should remain relatively negligible in comparison with the direct ice-uploaded suspended sediments (Eicken et al. 2005).

Isotopic analyses

In order to distinguish the detrital Pb isotopic composition, any anthropogenic Pb overprint has to be removed from sediment samples. For this purpose, surface sediment samples were wet sieved and their <100 μm fraction was treated following a procedure

Table 1. Location and isotopic composition of our samples. An expanded version of the table – with sample names, water depth and core depth – is available as Supplementary Table S2. Results with a high uncertainty are presented in italics.

Code name	Lat. (°N)	Long. (°E)	$^{87}Sr/^{86}Sr$	±	$^{144}Nd/^{143}Nd$	±	εNd	$^{208}Pb/^{204}Pb$	±	$^{207}Pb/^{204}Pb$	±	$^{206}Pb/^{204}Pb$	±
A1[a]	82.123	−102.583	0.723207	0.000014	0.512014	0.000010	−12.2	38.895	0.004	15.631	0.002	18.957	0.002
A2[a]	69.348	−137.987	0.730145	0.000014	*0.511878*	*0.000021*	−14.8	39.306	0.002	15.688	0.001	19.466	0.001
A3[b]	71.737	42.611	0.724660	0.000013	0.511884	0.000003	−14.7	38.622	0.009	15.597	0.003	18.672	0.005
A4[b]	73.048	58.949	0.723864	0.000017	0.511996	0.000019	−12.5	38.915	0.003	15.631	0.001	18.898	0.002
A5[a]	80.478	−102.606	0.722786	0.000009	0.511958	0.000017	−13.3	38.904	0.003	15.591	0.001	18.900	0.002
A6[a]	80.478	−102.606	0.722570	0.000024	0.511956	0.000007	−13.3	38.895	0.005	15.590	0.002	18.919	0.002
A7[c]	78.483	66.917	0.719432	0.000017	0.512146	0.000009	−9.6	38.777	0.000	15.605	0.000	18.798	0.000
A8[c]	81.420	77.925	0.718471	0.000015	*0.512097*	*0.000090*	−10.6	38.765	0.003	15.624	0.001	18.995	0.001
A9[a]	79.426	−107.255	0.723917	0.000018	0.511958	0.000008	−13.3	38.926	0.004	15.599	0.001	18.909	0.001
A10[a]	79.426	−107.255	0.723883	0.000014	0.511958	0.000006	−13.3	38.968	0.002	15.614	0.001	18.970	0.001
A11[a]	79.261	−102.199	0.724239	0.000010	0.511922	0.000004	−14.0	38.849	0.003	15.587	0.001	18.914	0.001
A12[a]	74.875	−106.413	0.738823	0.000020	0.511859	0.000010	−15.2	39.265	0.003	15.627	0.001	18.980	0.001
A13[d]	71.500	130.917	0.719365	0.000019	0.511993	0.000002	−12.6	38.747	0.003	15.579	0.001	18.697	0.004
A14[d]	71.922	160.033	0.711842	0.000012	0.512239	0.000008	−7.8	38.724	0.005	15.574	0.002	18.690	0.002
A15[d]	74.525	125.933	0.716291	0.000014	0.512033	0.000060	−11.8	–	–	–	–	–	–
A16[d]	74.525	125.933	0.718004	0.000009	*0.512065*	*0.000023*	−11.2	38.891	0.004	15.592	0.001	18.785	0.002
A17[d]	70.092	165.000	0.711724	0.000013	0.512180	0.000017	−8.9	38.682	0.000	15.562	0.000	18.635	0.000
A18[d]	74.317	138.967	0.715765	0.000009	0.511993	0.000002	−12.6	38.606	0.003	15.583	0.001	18.632	0.001
A19[d]	67.467	−170.367	0.710461	0.000011	0.512277	0.000011	−7.0	38.881	0.002	15.632	0.001	19.099	0.001
A20[a]	69.870	−133.973	0.730245	0.000011	0.511893	0.000009	−14.5	39.241	0.003	15.685	0.001	19.466	0.001
A21[a]	81.165	−96.092	0.724768	0.000009	0.511999	0.000009	−12.5	38.967	0.002	15.601	0.001	18.844	0.001
A22[d]	69.975	179.888	0.711931	0.000009	0.512199	0.000006	−8.6	38.830	0.003	15.603	0.001	18.953	0.001
A23[d]	73.750	133.883	0.715593	0.000009	0.511857	0.000010	−15.2	38.832	0.004	15.620	0.002	19.041	0.005
A24[d]	71.750	−156.500	0.712626	0.000009	0.512153	0.000008	−9.5	39.032	0.003	15.652	0.001	19.321	0.002
A25[d]	69.800	−165.500	0.711558	0.000011	0.512189	0.000017	−8.8	38.985	0.002	15.645	0.001	19.285	0.001
A29[d]	73.967	155.400	0.716451	0.000019	0.512090	0.000018	−10.7	38.804	0.003	15.582	0.001	18.715	0.001
A30[d]	72.583	149.500	0.714357	0.000007	0.511859	0.000011	−15.2	39.444	0.003	15.649	0.001	19.095	0.001
A31[d]	74.333	122.000	0.715230	0.000010	*0.512014*	*0.000026*	−12.2	38.526	0.003	15.583	0.001	18.689	0.002
A32[d]	70.450	175.000	0.711122	0.000011	0.512218	0.000012	−8.2	38.758	0.002	15.600	0.001	18.885	0.001
A33[d]	70.717	170.000	0.711612	0.000007	0.512259	0.000016	−7.4	38.681	0.004	15.580	0.001	18.753	0.002
A34[d]	75.500	120.000	0.714030	0.000012	0.511973	0.000006	−13.0	38.436	0.005	15.557	0.002	18.306	0.002
A35[d]	67.583	−173.408	0.711285	0.000014	0.512272	0.000009	−7.1	38.810	0.003	15.618	0.001	19.006	0.001
A36[d]	74.325	143.733	0.715311	0.000014	0.512011	0.000004	−12.2	38.667	0.002	15.582	0.001	18.611	0.001
A47[e]	84.807	40.599	0.727595	0.000026	0.512143	0.000014	−9.7	38.945	0.003	15.634	0.001	19.043	0.001
A48[e]	82.662	47.889	0.726424	0.000017	0.512019	0.00003	−12.1	38.910	0.003	15.618	0.001	18.915	0.001
A49[f]	79.574	25.838	0.737505	0.000018	0.512175	0.000029	−9.0	39.418	0.003	15.673	0.001	19.385	0.001
A50[f]	78.569	34.061	0.725399	0.000016	0.512073	0.000016	−11.0	39.008	0.003	15.644	0.001	19.095	0.001
A51[d]	81.621	−63.258	0.744196	0.000013	0.511639	0.000004	−19.5	38.735	0.004	15.610	0.002	18.968	0.002
A52[g]	79.617	−4.676	0.725988	0.000015	0.511824	0.000004	−15.9	–	–	–	–	–	–

[a] Bedford Institute of Oceanography. [b] Byrd Polar Research Center. [c] Antartic Research Facility, Florida State University. [d] Oregon State University. [e] Woods Hole Oceanographic Institution. [f] British Ocean Sediment Core Research Facility. [g] GEOMAR Helmholtz Centre for Ocean Research Kiel.

Table 2. Location and isotopic composition of sea-ice sediment samples.

Sample	Collection date	Grain size	Latitude (°N)	Longitude (°E)	$^{87}Sr/^{86}Sr$	±	$^{144}Nd/^{143}Nd$	±	εNd	$^{208}Pb/^{204}Pb$	±	$^{207}Pb/^{204}Pb$	±	$^{206}Pb/^{204}Pb$	±
SIS 2	29/9/2008	bulk	81.749	139.315	0.717898	0.000010	0.512033	0.000015	−11.8	38.6860	0.0011	15.5916	0.0005	18.6107	0.0006
SIS 3	29/9/2008	bulk	80.997	137.473	0.717080	0.000010	0.512015	0.000015	−12.2	38.5537	0.0010	15.6001	0.0004	18.5217	0.0004
HLY0901–21	-	bulk	62.728	−168.984	0.708923	0.000010	0.512343	0.000008	−5.8	38.8138	0.0017	15.6592	0.0007	19.1062	0.0009
HLY0901-36	-	bulk	62.725	−169.017	0.708838	0.000010	0.512342	0.000008	−5.8	38.8611	0.0010	15.6890	0.0004	19.2380	0.0005
LOMROG 4D+E	20/8/2007	<45 µm	87.615	10.073	0.714325	0.000019	0.512020	0.000008	−12.0	38.7035	0.0042	15.6111	0.0016	18.7467	0.0019
H1-6	18/6/2005	<45 µm	72.730	−156.317	0.716440	0.000013	0.512034	0.000009	−11.8	38.6038	0.0017	15.6858	0.0007	18.9590	0.0008
H1-11	23/6/2005	<45 µm	72.511	−156.949	0.714573	0.000014	*0.512178*	*0.000024*	*−9.0*	38.5769	0.0026	15.6070	0.0010	18.6550	0.0012
H3-2	29/8/2005	<45 µm	84.312	−149.085	0.716909	0.000010	0.512032	0.000011	−11.8	38.6948	0.0042	15.6157	0.0016	18.7144	0.0020
H3-7A	06/9/2005	<45 µm	87.623	156.087	0.716176	0.000009	0.512017	0.000009	−12.1	38.6995	0.0005	15.5905	0.0001	18.5647	0.0002
H3-8A	07/9/2005	<45 µm	87.663	150.874	0.717456	0.000014	0.512028	0.000010	−11.9	38.7263	0.0016	15.6352	0.0006	18.8369	0.0008
H3-11	13/9/2005	<45 µm	89.341	−86.137	0.717437	0.000017	0.512013	0.000009	−12.2	38.6900	0.0034	15.6475	0.0013	18.8749	0.0016

developed by Gutjahr et al. (2007). The <100 µm fraction was chosen primarily to avoid biases linked to very coarse grains discharged by icebergs, we decided to keep the fraction >63–100 µm as it might represent more than 20% of the total sediment in some cored sequences (Not & Hillaire-Marcel 2010). To not include the sand fraction would possibly mask some potential contributors, especially proximal and glacier sources, and hence over-represent sources and mechanisms mostly responsible for the dispersal and re-suspension of fine fractions. Samples were then leached with a Na–acetate buffer (1M Na acetate – 1M acetic acid; 52:48) to remove calcium carbonate. After rinsing, samples were leached with a 0.05M solution of hydroxylamine hydrochloride – 15% acetic acid – 0.03M Na–ethylenediaminetetraacetic acid (Na-EDTA) (buffered to pH 4) for 24 h at room temperature. This protocol is used to remove biogenic carbonates and Fe-Mn hydroxides assuming that the residual fraction is mainly silicates. However, our samples present large regional discrepancies, including the presence of detrital carbonates from northern Canada, mainly dolomitic (Parnell et al. 2007 and references therein). It is unlikely that this procedure has completely removed detrital dolomite particles as it is less easily dissolved (Hélie et al. 2009), hence the residual fraction analysed might contain both detrital silicates and dolomite. Hence, a significant presence of dolomite might influence the isotopic composition of our samples (trace elements in dolomite: Pb from 5 to 20 ppm; Nd from 10 to 100 ppm; Sr from 100 to 4000 ppm; James et al. 2001).

The residual sediment, i.e., the calcite- and metal oxide-free fraction, and sea-ice samples were digested and analysed for its radiogenic isotope content. It was first digested with an HF/HNO_3 acid mixture, then treated with aqua regia on a hot plate at 130°C. In order to extract Nd, the solution was passed through two sets of columns. A first column was filled with TRU Spec© resin. Diluted HNO_3 was used to separate rare earth elements and Sr-Rb. Nd was then isolated from other REE with diluted HCl, on Ln Spec© resin. Sr was purified through a two-pass ion exchange chromatography on Sr Spec© resin. Blanks for the Nd and Sr procedures were under 300 pg and 120 pg, respectively. Sr isotopes were measured with a Triton Plus™ instrument in static mode using a Ta activator (Birck 1986). $^{87}Sr/^{86}Sr$ ratios were normalized to $^{86}Sr/^{88}Sr = 0.1194$. Repeated analyses of standard SRM-987 yielded values of 0.710251 (± 0.000023, 2σ reproducibility over the course of this study, except when otherwise notified). Nd isotopes were analysed as Nd+ using the current double filament mounting, on the same thermal ionization mass spectrometer instrument as Sr. Mass fractionation was monitored using $^{146}Nd/^{144}Nd = 0.7219$. Replicate analyses of the standard JNdi-1 (Tanaka et al. 2000) yielded a mean value of $^{143}Nd/^{144}Nd = 0.512100$ (± 0.000015).

The Nd isotopic composition has been finally expressed as:

$$\varepsilon Nd = \left[\frac{(^{143}Nd/^{144}Nd)_{Sample}}{(^{143}Nd/^{144}Nd)_{CHUR}} - 1\right] * 10^4,$$

where CHUR stands for Chondritic Uniform Reservoir and represents a present day average Earth value $(^{143}Nd/^{144}Nd)_{CHUR}$ = 0.512638 (Jacobsen & Wasserburg 1980).

Pb was extracted through anion-exchange chromatography, following Manhès et al. (1980). Measurements were performed on a Nu Plasma II ™ MC-ICPMS. NIST 981 was used as reference material. Instrumental mass bias was corrected internally after addition of NIST Standard Reference Materials 997 Tl solution (White et al. 2000). Nominal isotopic values used for Pb and Tl ($^{205}Tl/^{203}Tl$ of 2.3889) reference materials, were taken from Thirlwall (2002). Internal analytical uncertainty was estimated by repeated measurement of the Pb-Tl reference material. NIST 981 Pb-ratios indicate an internal reproducibility better than 200 ppm/amu (2*sd of the mean: $^{208}Pb/^{206}Pb$: 2.16753 ± 0.00091; $^{207}Pb/^{206}Pb$: 0.91478 ± 0.00013; $^{208}Pb/^{204}Pb$: 36.724 ± 0.020; $^{207}Pb/^{204}Pb$: 15.4991 ± 0.0059; $^{206}Pb/^{204}Pb$: 16.9431 ± 0.0036). Blanks for the Pb procedure in detrital residues were under 180 pg. Replicate analyses yielded overall 2σ reproducibilities of ±0.3, ±0.03, ±0.1, ±0.002 and ±0.002 on the $^{208}Pb/^{204}Pb$, $^{207}Pb/^{204}Pb$, $^{206}Pb/^{204}Pb$, $^{208}Pb/^{206}Pb$ and $^{207}Pb/^{206}Pb$ ratios, respectively.

Results

Surface sediments

Radiogenic isotope data of surface sediments are discussed with reference to the geographical location of the samples (Figs. 1, 2). Six geographical areas have been

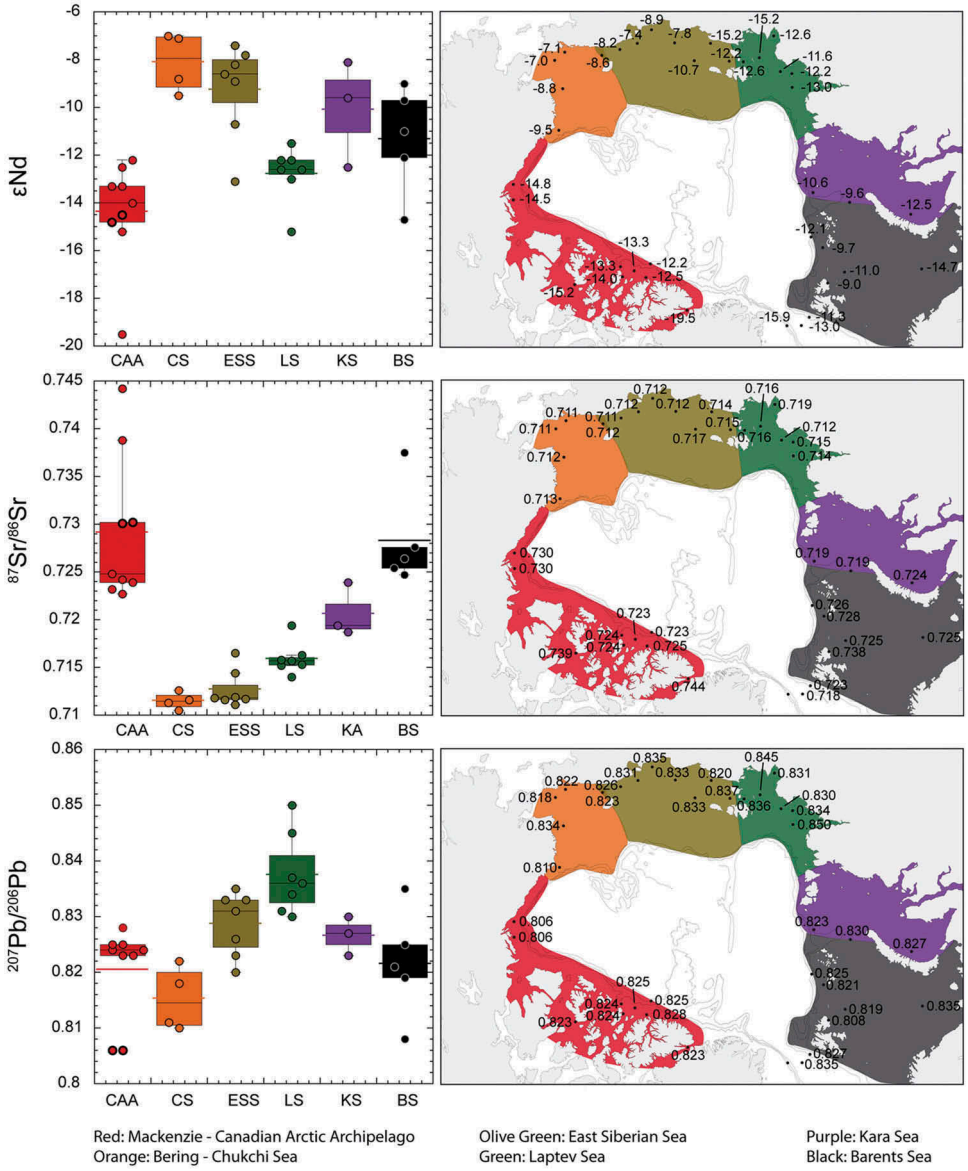

Figure 2. Isotopic ratios (left) and geographical distribution (right). The geographical zone have been defined regarding seas and drainage basins of the main river systems.

defined, corresponding mainly to drainage basins and their adjacent seas: the CAA, the CS, the ESS, the LS, the BS and KS. Samples have εNd values ranging from −19.5 to −7.0, $^{87}Sr/^{86}Sr$ ratios from 0.710 to 0.744, $^{208}Pb/^{204}Pb$ from 38.4 to 39.4, $^{207}Pb/^{204}Pb$ from 15.6 to 15.7 and $^{206}Pb/^{204}Pb$ from 18.3 to 19.5.

Sample spatial coverage in each region is variable, from three in the KS to nine in the combined Mackenzie delta region, Beaufort Sea continental margin, and CAA. Figure 2 shows the relative homogeneity/heterogeneity for each region as well as isotopic value overlaps. εNd values in the CS region have a total range of ca. 2.5 εNd units while it is up to ca. 6 εNd units for the ESS region. Similarly, for Sr isotopes there is an order of magnitude difference, with a total range of ca. 0.002 in the CS compared to ca. 0.02 in the CAA. $^{207}Pb/^{206}Pb$ ratios range within ca. 0.007 in the CS compared to ca. 0.02 in the LS.

Figure 2 also illustrates isotopic overlaps between the different regions. The CAA and BS cannot be distinguished as their compositions overlap in all three radiogenic systems of the present study (Figs. 3–6), whereas if the CS and ESS cannot be distinguished based solely on their Nd and Sr isotopic compositions (Fig. 3), they do present distinct Pb isotopic compositions (Figs. 4–6).

The Nd-Sr systematics have been widely used in the Arctic (e.g., Eisenhauer et al. 1999; Tütken et al. 2002; Guo et al. 2004). They are plotted in Fig. 3 along with data from the literature. The Bering, Chukchi and East Siberian seas samples occupy the top left corner of the diagram with the most radiogenic Nd values and the most unradiogenic Sr values, probably influenced by the Aleutian arc volcanism. Both CS and ESS samples overlap in this diagram and can't be clearly differentiated. Opposite, at the bottom right corner of Fig. 3, Nares Strait, CAA and Mackenzie samples present the most unradiogenic εNd values and the most radiogenic Sr ratios, likely reflecting material from the North American Craton. Samples from oceanic waters off the Mackenzie River delta present an isotopic composition similar to that of the Mackenzie suspended particulate matter (>0.2 µm; (Millot et al. 2004), while a sediment sample collected close of the Lena River mouth (N-42 from Guo et al. 2004) presents a somewhat different isotopic composition than suspended particulate matter from the Lena River itself (Millot et al. 2004). Kara, Barents and Laptev seas samples plot in between the two above-mentioned regions. Kara and Barents seas samples cannot be clearly identified as they overlap with other regions. In the Nd versus Pb space (Fig. 4), the Chukchi and East Siberian seas can be distinguished as CS samples and present a more radiogenic Pb composition. However, Kara and Barents seas samples cannot be distinguished because of overlaps with other regions. Finally, in the Sr versus Pb space (Fig. 5), Kara and Barents seas samples are still overlapping with either the CAA samples or the LS.

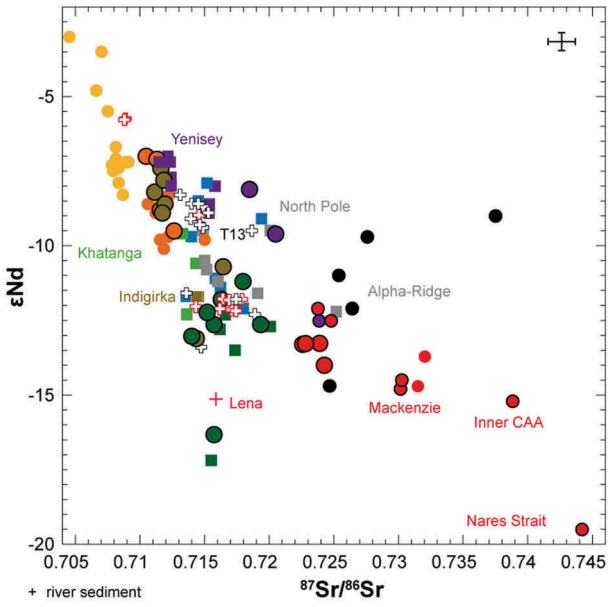

Figure 3. Nd versus Sr isotopes diagram. Error bars for our samples are represented in the upper right corner of the diagram. See key in Figs. 1 and 3. Data from the literature are from Winter et al. (1997) for Alpha Ridge, Guo et al. (2004) for Khatanga, Indigirka, Lena, Ob and Yenisey rivers, Haley et al. (2008) for the North Pole, Tütken et al. (2002) for sea ice and the LS, Eisenhauer et al. (1999) for the LS, Asahara et al. (2012) for the Bering, Chukchi and Beaufort seas, and Millot et al. (2004) for the Mackenzie and Lena rivers.

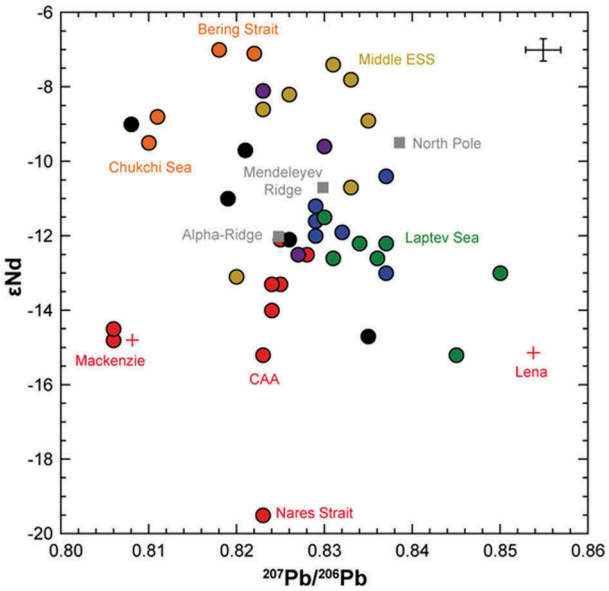

Figure 4. εNd *vs* $^{207}Pb/^{206}Pb$ isotopes diagram. See keys in Figs. 1 and 3. Error bars for our samples are represented in the top right corner of the diagram. Data from the literature are from Winter et al. (1997) for Alpha Ridge, Guo et al. (2004) for Khatanga, Indigirka, Lena, Ob and Yenisey rivers, Haley et al. (2008) for the North Pole, Tütken et al. (2002) for sea ice and the LS, Eisenhauer et al. (1999) for the LS, Asahara et al. (2012) for the Bering, Chukchi and Beaufort seas, and Millot et al. (2004) for the Mackenzie and Lena rivers.

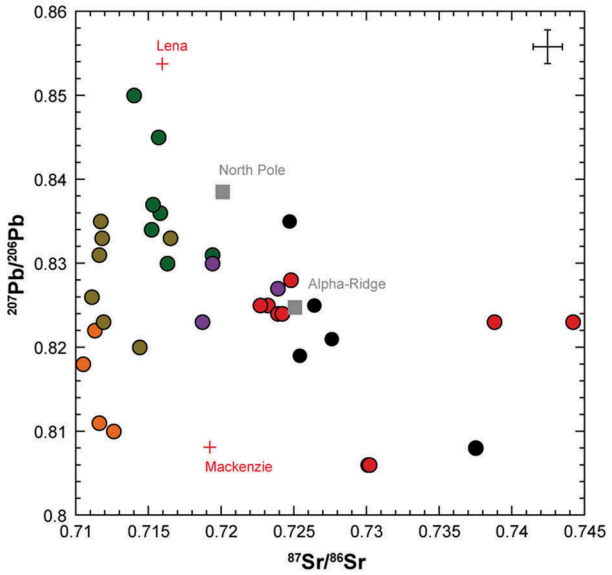

Figure 5. $^{207}Pb/^{206}Pb$ *vs* $^{87}Sr/^{86}Sr$ isotopes diagram. Error bars for our samples are represented in the top right corner of the diagram. See keys in Figs. 1 and 3. Data from the literature are from Winter et al. (1997) for Alpha Ridge, Guo et al. (2004) for Khatanga, Indigirka, Lena, Ob and Yenisey rivers, Haley et al. (2008) for the North Pole, Tütken et al. (2002) for sea-ice and the LS, Eisenhauer et al. (1999) for the LS, Asahara et al. (2012) for the Bering, Chukchi and Beaufort seas, and Millot et al. (2004) for the Mackenzie and Lena rivers.

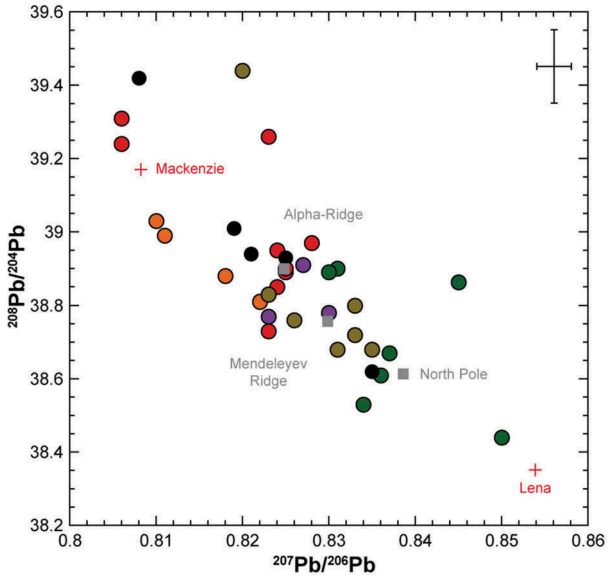

Figure 6. $^{208}Pb/^{204}Pb$ versus $^{207}Pb/^{206}Pb$ isotopes diagram. Error bars for our samples are represented in the top right corner of the diagram. See keys in Figs. 1 and 3. Data from the literature are from Winter et al. (1997) for Alpha Ridge, Guo et al. (2004) for Khatanga, Indigirka, Lena, Ob and Yenisey rivers, Haley et al. (2008) for the North Pole, Tütken et al. (2002) for sea-ice and the LS, Eisenhauer et al. (1999) for the LS, Asahara et al. (2012) for the Bering, Chukchi and Beaufort seas, and Millot et al. (2004) for the Mackenzie and Lena rivers.

Discriminant function analyses were attempted on the 35 samples of the present study: samples were split into six groups corresponding to the six geographical regions; combinations of two isotopic systems, or all three were tested. Results are presented in Table 3. A sample was considered misclassified if its group membership probability was <0.2 or if its probability of belonging to another group was higher than its group membership probability. Considering binary pairing of isotopes, 46–49% of samples were misclassified, regardless of the isotope combination. Even when adding data from the literature for the Nd-Sr systematics, 49% of samples were still misclassified (27 out of 56). When using all three isotopes, 23% of the samples were misclassified, which means that one out of four samples has an isotopic composition that does not match the region it belongs to. However, it is worth noting that out of the eight misclassified samples, three belong to the CAA.

Sea-ice samples

The two samples from the Bering Sea display the most radiogenic εNd values (−5.8) and Pb isotopic ratios ($^{208}Pb/^{204}Pb$ = 38.8, $^{207}Pb/^{204}Pb$ = 15.7 and $^{206}Pb/^{204}Pb$ = 19.2) and the least radiogenic $^{87}Sr/^{86}Sr$ ratio (ca. 0.7089). Samples from the central Arctic Basin present εNd values ranging from −12.2 to −9.0, $^{87}Sr/^{86}Sr$ ratios from 0.714 to 0.718, $^{208}Pb/^{204}Pb$ from 38.6 to 38.7, $^{207}Pb/^{204}Pb$ from 15.6 to 15.7 and $^{206}Pb/^{204}Pb$ from 18.5 to 19.0 (Table 2).

Discriminant function analysis was used again to match sea-ice sediment samples to circum-Arctic regions with regards to their isotopic composition (Table 4). The two samples from the Bering Sea present a CS membership/isotopic composition while samples from the central Arctic displays a Siberian shelf signature, mainly from the LS.

Discussion

Prior to examining further isotopic signatures in recent and modern Arctic Ocean sediments, a caveat seems needed. Samples were recovered from several repositories. They illustrate randomly distributed sites, unevenly spaced and with variable sedimentation rates. Nonetheless, the 35 study samples represent about a 50% increase on the available data about radiogenic isotope compositions of Arctic sediments (see Supplementary Table S1). Even when all available data are compiled, a few significant gaps remain, especially off the CAA and off northern Greenland (Fig. 1). Similarly, ridge as well as ice-transported sediments are scarcely and randomly distributed. Grain-size differences might also influence isotopic compositions (Eisenhauer et al. 1999; Nørgaard-Pedersen et al. 2003; Schmitt 2007). All statistical analyses made here were performed on <100 μm fractions, reducing the impact of very coarse elements. Comparisons with bulk sediment cannot be discarded, however. They simply bear some larger uncertainty (Saukel et al.

Table 3. Results of discriminant function analyses. Asterisks correspond to misclassified samples.

	Two isotopic systems			Three isotopic systems	
	Nd, Sr	Nd, Pb	Sr, Pb	Nd, Sr, Pb	Nd, Sr, Pb without CAA
A1	*	*	*	*	
A2					
A3	*	*	*	*	
A4	*	*	*	*	*
A5/A6	*	*	*		
A7		*			
A8		*			
A9/A10		*	*		
A11			*		
A12				*	
A13			*		
A14	*				
A15/A16		*	*	"	
A17	*		*		
A18					
A19					
A20					
A21	*	*	*	*	
A22	*	*	*	*	*
A23					
A24	*				
A25	*				
A29	*	*	*	*	*
A30	*	*			
A31		*	*		
A32	*	*			
A33	*				
A34					
A35					
A36					
A47		*	*		
A48	*	*	*		
A49		*	*		
A50	*		*		
A51					
Number misclassified	16	17	17	8	3
Percent misclassified	45.7	48.6	48.6	22.9	11.5
Entropy Rsquare	0.56275	0.49818	0.5696	0.69755	0.84
"-2 log-likelihood"	52.935	60.7518	52.1056	36.6151	12.9843

2010; Gamboa et al. 2017) than those made on sieved fractions. Nevertheless, the assembled database (Table 1) highlights a few robust features that might be critical when using radiogenic isotopes for the documenting of sedimentological regimes in the Arctic palaeocean.

Discriminant function analyses

Statistical analysis have already been used on Fe-oxide grains in Arctic Ocean sediments by Darby et al. (2003)

Table 4. Discriminant function analysis results for sea-ice sediment samples.

Samples	Source	Probability	Other
SIS 2	LS	0.6713	ESS 0.13 KS 0.18
SIS 3	LS	0.8416	
HLY09-01-21	CS	0.8266	ESS 0.16
HLY0901-36	CS	0.9554	
LOMROG 4D+E	LS	0.6442	ESS 0.26
H1-6	KS	0.3281	CS 0.16 ESS 0.20 LS 0.23
H1-11	KS	0.423	ESS 0.41 LS 0.15
H3-2	LS	0.571	ESS 0.20 KS 0.20
H3-7A	LS	0.8336	ESS 0.11
H3-8A	LS	0.4123	ESS 0.23 KS 0.29
H3-11	LS	0.4114	ESS 0.19 KS 0.28

to highlight sediment sources and transport. Here we have used a similar approach using radiogenic isotopes and to our knowkedge this is the first study reporting such statistical results to trace continental sources in oceanic settings. Discriminant function analysis highlights the fact that there are overlaps between the different shelf areas. When considering any combination of two isotopic systems, one out of two samples is misclassified, i.e., the source areas cannot be isotopically sorted. When using the three isotopic systems, the misclassified samples fall down to about one out of four, with about a 23% chance that a sample yields isotopic composition fitting with another source area. Most of this uncertainty is due to isotopic overlaps between the CAA area and the BS and KS areas. It might also result from isotopic heterogeneities within source areas, or active redistribution mechanisms over Arctic continental margins (e.g., sea ice), or possibly to the limited number of samples used to run the discriminant function analysis. Larger data set and/or other tracers would surely improve the analysis.

When removing the CAA region, i.e., when considering Siberian seas only, the misclassified sample number decreases to ca. 11% using the three isotopic

systems. Within the Siberian sector, from the BS to the CS, relatively well clustered signatures are observed between areas.

Regional isotopic signatures

At any given location, sedimentary inputs include (i) continental inputs through land drainage, (ii) coastal erosion products and (iii) distal material transported by currents and sea ice (Stein 2008; Macdonald & Gobeil 2012; Macdonald et al. 2015; Wegner et al. 2015). The Beaufort Gyre and the Trans-Polar Drift – the two main surface current systems in the Arctic – redistribute sea ice over the Arctic Basin. In addition to the Beaufort Gyre and the Trans-Polar Drift, shelf currents (Naugler et al. 1974; Weingartner et al. 1999) might redistribute sediment over the Arctic shelves (Fig. 1).

The Kara and Barents seas consist of large continental margins, spanning more than 10° latitude (>1000 km). Within the representative samples, A3 and A4 at the south-end of the continental margin, i.e., closest to the continent, present unradiogenic εNd values (Table 1), maybe linked to inputs from old formations from the northern Scandinavian Precambrian Craton and Novaya Zemlaya. Sample A49, close to the island of Nordauslandet in the archipelago of Svalbard (Fig. 1), presents a specific isotopic composition, likely highlighting local inputs from Nordaustlandet. The local inputs seem to be spatially restricted as the nearby sample A50 (approximately 200 km apart) displays a distinct isotopic composition. Otherwise, neither the KS nor the BS show distinct isotopic compositions, but a large overlap, hampering any unequivocal inference about sediment provenance on such grounds. However the large scatter of isotopic values suggests several distinct sediment sources, with possibly active redistribution mechanisms.

Along the ESS and the LS, a sediment plume is clearly visible from satellite observation along the coastline, suggesting intense coastal erosion (Vonk et al. 2012). In this area, most samples were collected near the coastline and should capture both coastal and land drainage signals. Samples A13, A23 and A15 are the closest to the Lena River mouth (ca. 100–150 km). These samples present an isotopic composition differing significantly from that of the Lena River suspended particulate matter (Figs. 3–6), highlighting the overall weak linkage of radiogenic isotope signatures of coastal sediment to inland sources. On the western side of the LS, coastal terrains are mostly of Cenozoic ages, while those on the eastern side are of Late Palaeozoic and Cenozoic ages, but no clear isotopic trend can be identified in representative samples. Similarly, the LS samples from the present study and literature (Eisenhauer et al. 1999; Guo et al. 2004) present a large scatter of Nd-isotope values, despite the proximity of the Lena River delta. They range from εNd −17.2 to −11.5, indicating a strong buffering offshore of unradiogenic Nd signatures from the Lena River by other supplies. Processes leading to this scatter are open to discussion, but oceanic currents and sea-ice growth and dispersal are likely to play a role. Nevertheless, the relatively dense sample distribution in the LS allows for the differentiation of proximal versus distal shelf areas, as Darby et al. (2003) suggested on the basis of mineralogical criteria. The outer shelf area displays higher εNd values, due to enhanced mixing of the material bearing a Lena River signature, with material transported by sea ice and currents from remote areas, in particular the KS (Darby 2003).

The ESS coast presents Cenozoic formations westward, and Mesozoic formations eastwards and as far as the CS, with – locally – upper Palaeozoic rocks in front of Wrangel Island. Sr and Pb compositions define a trend along the coast from the middle ESS, with both $^{87}Sr/^{86}Sr$ and $^{207}Pb/^{206}Pb$ ratios decreasing eastwards. This might reflect mixing of sediments either via oceanic currents and/or sea-ice redistribution along the coast between the CS and the ESS (Naugler et al. 1974). In the ESS shelf, samples A17, A14 and A33 define a relatively homogeneous group (Figs. 4–6) and likely reflect some local coastal inputs, probably mixed with distal material from both the Laptev and Chukchi seas via coastal currents, as previously suggested by (Schoster et al. 2000; Viscosi-Shirley et al. 2003) based on mineralogical features.

In the CS, samples A19 and A35 present isotopic composition close to those of nearby samples from the ESS, suggesting some physical transport of sediments along the shelf. The two other samples from the CS (A24 and A25), closer to the Alaskan coast, present isotopic compositions intermediate with those from the Mackenzie area (Figs. 3–6) and might be interpreted as a westward contribution from the Mackenzie region to the CS, as previously suggested by Darby et al. (2003).

Off the CAA, samples A2 and A20 located off the Mackenzie River mouth (about 100 km away), present isotopic compositions quite similar to those of the Mackenzie River suspended particulate matter, clearly reflecting dominant Mackenzie River inputs in the area (Millot et al. 2004). Eastwards, the five samples off Ellesmere Island display quite clustered isotopic compositions. Interestingly, a bulk sediment sample (Figs. 3–6) from Alpha Ridge (Winter et al. 1997) also yielded an isotopic composition similar to those obtained here on sediment residues from the CAA shelf. This might indicate some contributions from the Canadian shelf to the central Arctic via the Beaufort Gyre. Sample A12, south of Melville Island, presents more unradiogenic εNd and radiogenic Sr ratios than other CAA samples. Given the fact that ocean currents flow south-eastward through the archipelago, sample A12 likely records some influence of pre-Cambrian shield rocks superimposed on

more local Palaeozoic supplies (Fig. 1). Finally, sample A51 displays the most unradiogenic εNd value, and the most radiogenic $^{87}Sr/^{86}Sr$, likely reflecting old formations from Ellesmere Island and northern Greenland.

River and land drainage signatures

With reference to direct river supplies, a Mackenzie isotopic signature is clearly present in sediments from the Beaufort Sea. In contrast, the Lena River signal cannot be clearly identified based on the available data set and hence does not appear to be the main provider of sediments to the LS. This can be explained by the sedimentary budget of the Mackenzie River versus the Lena River. Indeed, based on estimates from Stein (2008) the Mackenzie River sedimentary discharge is four time higher than that of the Lena River. In addition, coastal erosion is negligible along the Beaufort Sea while it accounts for two-thirds of the sediment supply in the LS, and more generally along the Siberian seas.

Sea-ice sediments

Sea ice is responsible for proximal to distal redistribution of sedimentary material over the Arctic Ocean (Darby 2003; Macdonald et al. 2015). A few sea-ice sediment samples could be analysed within the framework of the present study. Of course, the time frames recorded in shelf versus sea-ice sediment samples differ by orders of magnitude. Samples from marine surface sediments may represent several hundreds to thousands of years (e.g., Barletta et al. 2010; Not & Hillaire-Marcel Claude 2010; Rudenko et al. 2014). Samples from sea-ice represent a single sea-ice growth season up to – in the case of multi-year ice – a few years, the sea-ice growth season in many cases. Modern sea-ice circulation is controlled by the Beaufort Gyre and the Trans-Polar Drift, themselves governed by atmospheric conditions (Serreze & Barry 2005) inducing an inherent high-frequency drift variability. Sea-ice sediment samples analysed here (Fig. 1, Table 2, Supplementary Table S1) were collected during three years (2005, 2007 and 2008) in the central Arctic Ocean, the Bering Sea and the western Arctic. We used discriminant function analysis to identified sea-ice sediment sources (Table 4). Sea-ice sediment collected in the central Arctic (SIS 2, SIS 3, LOMROG 4D+E, H3-2, H3-7A, H3-8A, H3-11) seems to mainly originate from the LS, with possible minor contributions from the KS and the ESS. The two samples from the Bering Sea (HLY09-01-21 and HLY09-01–36) present a robust CS isotopic signature, whereas the two samples from the western Arctic (H1-6 and H1-11), close to the Alaskan coast, indicate multiple and distinct sources: sample H1-6 presents significant contributions from the Kara, Laptev and East Siberian seas, whereas sample H1-11 displays contributions from both the KS and the ESS, suggesting some rerouting of carrier ice rafts from the Trans-Polar Drift through the Beaufort Gyre. These two samples have been collected during different years and illustrate the high variability in sea-ice recirculation. Nevertheless, most sea-ice data point to a dominant LS isotopic signature, which suggests that sea-ice formation and sediment entrainment occurs mainly in this area as documented elsewhere (Pfirman et al. 1997). Our isotopic results differ slightly from Fe-oxide grains source identification (Darby 2003): no contribution from Banks island (i.e., CAA) was identified in the present study samples, possibly due to the small number of samples available in comparison to Darby et al. (2003). In contrast, a minor ESS contribution has been found in several sea-ice samples (Table 4) but was not recognized in previous studies despite the fact that this area seems favourable for sediment entrainment on account of its shallowness and large extent.

Palaeoceanographic perspectives

Sedimentary and weathering fluxes are likely to have varied through time in response to hydro-climatic and topographic changes during terminations, i.e., from each ice age to the following interglacial. Under full glacial conditions, for example, during the Last Glacial Maximum, when mean sea level was more than 120 m below its present level (Bard et al. 1990), conditions were drastically distinct. The Arctic Ocean was half its actual size and its shelves, where modern sea-ice factories are located, were exposed, hampering sea-ice formation and sediment incorporation into it. Sedimentary supplies were then closely associated with continental ice erosional products, ice-sheet streaming routes and ice-margin instabilities (e.g., Stokes & Clark 2001; Maccali et al. 2013), notably along the Canadian Arctic (Laurentide Ice Sheet) and the Bering–Kara seas shelf edge (Eurasian ice-complex; Hillaire-Marcel et al. 2013; Maccali et al. 2013). Prior to the Last Glacial Maximum, variations in the dynamics of these ice sheets (Siegert & Marsiat 2001), changes in relative sea levels around the Arctic Ocean and the relative closure/opening of Bering Strait are variables that cannot be ignored when interpreting radiogenic isotope data in Arctic Ocean sedimentary records. During interglacials, land–ocean fluxes and sea-ice regimes have also likely varied during and between each of them in relation with distinct atmospheric conditions, ice drifting patterns and sea-ice factory locations (e.g., De Vernal & Hillaire-Marcel 2008). In addition, whereas recent glacial intervals may have yielded consistent signatures in relation with the

development of the Laurentide and Eurasian ice sheets, other ice sheets might have interfered during earlier glaciations (Niessen et al. 2013). The isotopic signatures and sources identified above reflect modern conditions: the present geography of the Arctic Ocean, the present relative sea level and shelf extension, the present erosional regimes on land and along coastal areas, the present freshwater outlets and sea-ice factories and their export routes. Interpreting past interglacial sedimentary fluxes based on modern conditions should be done with caution.

Conclusions

Sediments from continental margins of the Arctic Ocean present a large range of isotopic composition, spanning ca. 13 εNd units, and ratio spans of ca. 0.035 and ca. 0.05 for $^{87}Sr/^{86}Sr$ and $^{207}Pb/^{206}Pb$, respectively. These radiogenic isotope composition illustrate a complex combination of land versus coastal erosion but also mixing and redistributing mechanisms of sediment via sea-ice routes and oceanic currents. Based on the present study data set, two-isotope systematics might introduce large uncertainty (ca. 50%) for modern source identification of surface and sea-ice transported sediments. However, combining Nd, Sr and Pb isotope data allows us to label circum-Arctic sources with a lesser uncertainty of about 23%, mainly accounted for by isotopic overlaps between the CAA and the Barents–Kara seas areas. River and coastal erosion inputs cannot be differentiated, with the exception of the Beaufort Sea–Mackenzie River system, possibly because of active coastal erosion inputs and active mixing mechanisms over the Siberian shelves. In the LS, where sample density was high, it has been possible to capture slight isotopic differences between the inner versus outer shelf, as previously reported by Darby & Bischof (1996). The few sea-ice sediment samples from the central Arctic Ocean available for this study are dominated by LS contributions, suggesting active sea-ice formation and sediment entrainment in the region. In addition, non-negligible contributions from the Kara and East Siberian seas were also recorded, reflecting the dynamics of sea-ice circulation over the Arctic Ocean.

Acknowledgements

The material used in this study was provided by Dr Dennis Darby (Old Dominion University), Dr Leonid Polyak (Byrd Polar Research Center, Ohio State University), Dr Charlotte Sjunneskog (Antarctic Research Facility, Florida State University), Mysti Weber (Oregon State University), James Broda and Ellen Roosen (Woods Hole Oceanographic Institution) and Suzanne MacLachlan (British Ocean Sediment Core Research Facility, National Oceanography Centre). M. Preda (Department of Earth and Atmospheric Sciences, Université du Québec à Montréal) is also thanked for his help with x-ray mineralogical analysis, as is Laure Meynadier, at (Institut de Physique du Globe de Paris) for her help with Sr, Pb and Nd isotope analyses on sea-ice sediments. We thank Professor Laodong Guo (University of Wisconsin–Milwaukee) for providing table data. We must also thank Dr Marcus Gutjahr (GEOMAR, Germany) for many useful comments on an earlier version of the manuscript and the three anonymous reviewers of the paper who contributed constructive comments.

Disclosure statement

No potential conflict of interest was reported by the authors.

Funding

This study has been financially supported by funds from the Québec Government (Fonds de Recherche du Québec – Nature et technologies – Equipe) and the Natural Sciences and Engineering Research Council of Canada (Discovery Grant grant to CHM).

ORCID

Christelle Not http://orcid.org/0000-0002-1386-6079

References

Asahara Y., Takeuchi F., Nagashima K., Harada N., Yamamoto K., Oguri K. & Tadai O. 2012. Provenance of terrigenous detritus of the surface sediments in the Bering and Chukchi seas as derived from Sr and Nd isotopes: implications for recent climate change in the Arctic regions. *Deep Sea Research Part II: Topical Studies in Oceanography 61–64*, 155–171.

Bard E., Hamelin B. & Fairbanks R.G. 1990. U-Th ages obtained by mass spectrometry in corals from Barbados: sea level during the past 130,000 years. *Nature 346*, 456–458.

Barletta F., St-Onge G., Channell J.E.T. & Rochon A. 2010. Dating of Holocene western Canadian Arctic sediments by matching paleomagnetic secular variation to a geomagnetic field model. *Quaternary Science Reviews 29*, 2315–2324.

Birck J.L. 1986. Precision KRbSr isotopic analysis: application to RbSr chronology. *Chemical Geology 56*, 73–83.

Darby D.A. 2003. Sources of sediment found in sea ice from the western Arctic Ocean, new insights into processes of entrainment and drift patterns. *Journal of Geophysical Research—Oceans 108*, article no. 3257, doi: 10.1029/2002JC001350

Darby D.A. & Bischof J.F. 1996. A statistical approach to source determination of lithic and Fe oxide grains: an example from the Alpha Ridge, Arctic Ocean. *Journal of Sedimentary Research 66*, 599–607.

Darby D.A. & Bischof J.F. 2004. A Holocene record of changing Arctic Ocean ice drift analogous to the effects of the Arctic Oscillation. *Paleoceanography 19*, PA1027, doi: 10.1029/2003PA000961

Darby D.A., Myers W., Herman S. & Nicholson B. 2015. Chemical fingerprinting, a precise and efficient method to determine sediment sources. *Journal of Sedimentary Research 85*, 247–253.

Darby D.A., Myers W.B., Jakobsson M. & Rigor I. 2011. Modern dirty sea ice characteristics and sources: the role of anchor ice. *Journal of Geophysical Research—Oceans 116*, C09008, doi: 10.1029/2010JC006675

De Vernal A. & Hillaire-Marcel C. 2008. Natural variability of Greenland climate, vegetation, and ice volume during the past million years. *Science 320*, 1622–1625.

Eicken H., Gradinger R., Gaylord A., Mahoney A., Rigor I. & Melling H. 2005. Sediment transport by sea ice in the Chukchi and Beaufort seas: increasing importance due to changing ice conditions? *Deep Sea Research Part II: Topical Studies in Oceanography 52*, 3281–3302.

Eisenhauer A., Meyer H., Rachold V., Tütken T., Wiegand B., Hansen B.T., Spielhagen R.F., Lindemann F. & Kassens H. 1999. Grain size separation and sediment mixing in Arctic Ocean sediments: evidence from the strontium isotope systematic. *Chemical Geology 158*, 173–188.

Fagel N., Not C., Gueibe J., Mattielli N. & Bazhenova E. 2014. Late Quaternary evolution of sediment provenances in the central Arctic Ocean: mineral assemblage, trace element composition and Nd and Pb isotope fingerprints of detrital fraction from the northern Mendeleev Ridge. *Quaternary Science Reviews 92*, 140–154.

Gamboa A., Montero-Serrano J.C., St-Onge G., Rochon A. & Desiage P.A. 2017. Mineralogical, geochemical, and magnetic signatures of surface sediments from the Canadian Beaufort Shelf and Amundsen Gulf (Canadian Arctic). *Geochemistry, Geophysics, Geosystems 18*, 488–512.

Goldstein S.L. & Hemming S.R. 2003. Long-lived isotopic tracers in oceanography, paleoceanography, and ice-sheet dynamics. In H.D. Holland & K.K. Turekian (eds.): *Treatise on geochemistry*. Pp. 453–489. Oxford: Pergamon.

Goldstein S.L., O'Nions R.K. & Hamilton P.J. 1984. A Sm-Nd isotopic study of atmospheric dusts and particulates from major river systems. *Earth and Planetary Science Letters 70*, 221–236.

Guo L., Semiletov I., Gustafsson Ö., Ingri J., Andersson P., Dudarev O. & White D. 2004. Characterization of Siberian Arctic coastal sediments: implications for terrestrial organic carbon export. *Global Biogeochemical Cycles 18*, GB1036, doi: 10.1029/2003GB002087

Gutjahr M., Frank M., Stirling C.H., Klemm V., van de Flierdt T. & Halliday A.N. 2007. Reliable extraction of a deepwater trace metal isotope signal from Fe-Mn oxyhydroxide coatings of marine sediments. *Chemical Geology 242*, 351–370.

Haley B.A., Frank M., Spielhagen R.F. & Fietzke J. 2008. Radiogenic isotope record of Arctic Ocean circulation and weathering inputs of the past 15 million years. *Paleoceanography 23*, PA1S13, doi: 10.1029/2007PA001486

Harrison J.C., St-Onge M.R., Petrov O., Strelnikov S., Lopatin B., Wilson F., Tella S., Paul D., Lynds T., Shokalsky S., Hults C., Bergman S., Jepsen H.F. & Solli A. 2008. *Geological map of the Arctic. Geological Survey of Canada. Open File 5816*. Ottawa: Geological Survey of Canada.

Hélie J.-F. 2009. Elemental and stable isotopic approaches for studying the organic and inorganic carbon components in natural samples. In C. Veiga-Pires & G. St-Onge (eds.): *From deep-sea to coastal zones: methods and techniques for studying paleoenvironments. IOP Conference Series: Earth and Environmental Science 5*, article no. 012005, doi: 10.1088/1755-1307/5/1/012005

Hillaire-Marcel C., Maccali J., Not C. & Poirier A. 2013. Geochemical and isotopic tracers of Arctic sea ice sources and export with special attention to the Younger Dryas interval. *Quaternary Science Reviews 79*, 184–190.

Jacobsen S.B. & Wasserburg G.J. 1980. Sm-Nd isotopic evolution of chondrites. *Earth and Planetary Science Letters 50*, 139–155.

James N.P., Narbonne G.M. & Kyser T.K. 2001. Late Neoproterozoic cap carbonates: Mackenzie Mountains, northwestern Canada: precipitation and global glacial meltdown. *Canadian Journal of Earth Sciences 38*, 1229–1262.

Knies J., Nowaczyk N., Müller C., Vogt C. & Stein R. 2000. A multiproxy approach to reconstruct the environmental changes along the Eurasian continental margin over the last 150 000 years. *Marine Geology 163*, 317–344.

Maccali J., Hillaire-Marcel C., Carignan J. & Reisberg L.C. 2012. Pb-isotopes and geochemical monitoring or Arctic sedimentary supplies and water-mass export through Fram Strait since the Last Glacial Maximum. *Paleoceanography 27*, PA1201, doi: 10.1029/2011PA002152

Maccali J., Hillaire-Marcel C., Carignan J. & Reisberg L.C. 2013. Geochemical signatures of sediments documenting Arctic sea-ice and water mass export through Fram Strait since the Last Glacial Maximum. *Quaternary Science Reviews 64*, 136–151.

Macdonald R.W. & Gobeil C. 2012. Manganese sources and sinks in the Arctic Ocean with reference to periodic enrichments in basin sediments. *Aquatic Geochemistry 18*, 565–591.

Macdonald R.W., Kuzyk Z.Z.A. & Johannessen S.C. 2015. The vulnerability of Arctic shelf sediments to climate change. *Environmental Reviews 23*, 461–479.

Manhes G., Allègre C.J., Dupré B. & Hamelin B. 1980. Lead isotope study of basic-ultrabasic layered complexes: speculations about the age of the Earth and primitive mantle characteristics. *Earth and Planetary Science Letters 47*, 370–382.

Millot R., Allègre C.J., Gaillardet J. & Roy S. 2004. Lead isotopic systematics of major river sediments: a new estimate of the Pb isotopic composition of the Upper Continental Crust. *Chemical Geology 203*, 75–90.

Naugler F.P., Silverberg N. & Creager J.S. 1974. Recent sediments of the East Siberian Sea. In Y. Herman (ed.): *Marine geology and oceanography of the Arctic seas*. Pp. 191–210. Berlin: Springer.

Navarro-Rodriguez A., Belt S.T., Knies J. & Brown T.A. 2013. Mapping recent sea ice conditions in the Barents Sea using the proxy biomarker IP25: implications for palaeo sea ice reconstructions. *Quaternary Science Reviews 79*, 26–39.

Niessen F., Hong J.K., Hegewald A., Matthiessen J., Stein R., Kim H., Kim S., Jensen L., Jokat W., Nam S.I. & Kang S.H. 2013. Repeated Pleistocene glaciation of the East Siberian continental margin. *Nature Geoscience 6*, 842–846.

Nørgaard-Pedersen N., Spielhagen R.F., Erlenkeuser H., Grootes P.M., Heinemeier J. & Knies J. 2003. Arctic Ocean during the Last Glacial Maximum: Atlantic and polar domains of surface water mass distribution and ice cover. *Paleoceanography 18*, article no. 1063, doi: 10.1029/2002PA000781

Not C. & Hillaire-Marcel Claude C. 2010. Time constraints from ^{230}Th and ^{231}Pa data in late Quaternary, low sedimentation rate sequences from the Arctic Ocean: an

example from the northern Mendeleev Ridge. *Quaternary Science Reviews 29*, 3665–3675.

Parnell J., Bowden S., Andrews J.T. & Taylor C. 2007. Biomarker determination as a provenance tool for detrital carbonate events (Heinrich events?): fingerprinting Quaternary glacial sources into Baffin Bay. *Earth and Planetary Science Letters 257*, 71–82.

Peucker-Ehrenbrink B., Miller M.W., Arsouze T. & Jeandel C. 2010. Continental bedrock and riverine fluxes of strontium and neodymium isotopes to the oceans. *Geochemistry, Geophysics, Geosystems 11*, Q03016, doi: 10.1029/2009GC002869

Pfirman S.L., Colony R., Nürnberg D., Eicken H. & Rigor I. 1997. Reconstructing the origin and trajectory of drifting Arctic sea ice. *Journal of Geophysical Research—Oceans 102*, 12575–12586.

Phillips R.L. & Grantz A. 2001. Regional variations in provenance and abundance of ice-rafted clasts in Arctic Ocean sediments: implications for the configuration of late Quaternary oceanic and atmospheric circulation in the Arctic. *Marine Geology 172*, 91–115.

Rachold V., Eicken H., Gordeev V.V., Grigoriev M.N., Hubberten H.W., Lisitzin A.P., Shevchenko V.P. & Schirrmeister L. 2004. Modern terrigenous organic carbon input to the Arctic Ocean. In R. Stein & R.W. MacDonald (eds.): *The organic carbon cycle in the Arctic Ocean*. Pp. 33–55. Berlin: Springer.

Reimnitz E., Dethleff D. & Nürnberg D. 1994. Contrasts in Arctic shelf sea-ice regimes and some implications: Beaufort Sea versus Laptev Sea. *Marine Geology 119*, 215–225.

Rudenko O., Tarasov P.E., Bauch H.A. & Taldenkova E. 2014. A Holocene palynological record from the northeastern Laptev Sea and its implications for palaeoenvironmental research. *Quaternary International 348*, 82–92.

Saukel C., Stein R., Vogt C. & Shevchenko V.P. 2010. Clay-mineral and grain-size distributions in surface sediments of the White Sea (Arctic Ocean): indicators of sediment sources and transport processes. *Geo-Marine Letters 30*, 605–616.

Schmitt W. 2007. *Application of the Sm-Nd isotope system to the late Quaternary paleoceanography of the Yermak Plateau (Arctic Ocean)*. Munich: Faculty of Geosciences. Ludwig-Maximilian University of Munich.

Schoster F., Behrends M., Müller C., Stein R. & Wahsner M. 2000. Modern river discharge and pathways of supplied material in the Eurasian Arctic Ocean: evidence from mineral assemblages and major and minor element distribution. *International Journal of Earth Sciences 89*, 486–495.

Serreze M.C. & Barry R.G. 2005. *The Arctic climate system*. Cambridge: Cambridge University Press.

Siegert M.J. & Marsiat I. 2001. Numerical reconstructions of LGM climate across the Eurasian Arctic. *Quaternary Science Reviews 20*, 1595–1605.

Stein R. 2008. Modern physiography, hydrology, climate, and sediment input. In: S. Ruediger (ed.): *Arctic Ocean sediments: processes, proxies, and paleoenvironment*. Pp. 35–84. Amsterdam: Elsevier.

Stokes C.R. & Clark C.D. 2001. Palaeo-ice streams. *Quaternary Science Reviews 20*, 1437–1457.

Tanaka T., Togashi S., Kamioka H., Amakawa H., Kagami H., Hamamoto T., Yuhara M., Orihashi Y., Yoneda S., Shimizu H., Kunimaru T., Takahashi K., Yanagi T., Nakano T., Fujimaki H., Shinjo R., Asahara Y., Tanimizu M. & Dragusanu C. 2000. JNdi-1: a neodymium isotopic reference in consistency with LaJolla neodymium. *Chemical Geology 168*, 279–281.

Thirlwall M.F. 2002. Multicollector ICP-MS analysis of Pb isotopes using a ^{207}Pb-^{204}Pb double spike demonstrates up to 400 ppm/amu systematic errors in TI-normalization. *Chemical Geology 184*, 255–279.

Tütken T., Eisenhauer A., Wiegand B. & Hansen B.T. 2002. Glacial–interglacial cycles in Sr and Nd isotopic composition of Arctic marine sediments triggered by the Svalbard/Barents Sea ice sheet. *Marine Geology 182*, 351–372.

Viscosi-Shirley C., Mammone K., Pisias N. & Dymond J. 2003. Clay mineralogy and multi-element chemistry of surface sediments on the Siberian-Arctic shelf: implications for sediment provenance and grain size sorting. *Continental Shelf Research 23*, 1175–1200.

Vogt C. & Knies J. 2008. Sediment dynamics in the Eurasian Arctic Ocean during the last deglaciation – the clay mineral group smectite perspective. *Marine Geology 250*, 211–222.

Vonk J.E., Sánchez-García L., Van Dongen B.E., Alling V., Kosmach D., Charkin A., Semiletov I.P., Dudarev O.V., Shakhova N., Roos P., Eglinton T.I., Andersson A. & Gustafsson A. 2012. Activation of old carbon by erosion of coastal and subsea permafrost in Arctic Siberia. *Nature 489*, 137–140.

Wahsner M. 1999. Clay-mineral distribution in surface sediments of the Eurasian Arctic Ocean and continental margin as indicator for source areas and transport pathways – a synthesis. *Boreas 28*, 215–233.

Wegner C., Bennett K.E., De Vernal A., Forwick M., Fritz M., Heikkilä M., Łącka M., Lantuit H., Laska M., Moskalik M., Regan M., Pawłowska J., Promińska A., Rachold V., Vonk J.E. & Werner K. 2015. Variability in transport of terrigenous material on the shelves and the deep Arctic Ocean during the Holocene. *Polar Research 34*, article no. 24964, doi: 10.3402/polar.v34.24964

Weingartner T.J., Danielson S., Sasaki Y., Pavlov V. & Kulakov M. 1999. The Siberian Coastal Current: a wind- and buoyancy-forced Arctic coastal current. *Journal of Geophysical Research—Oceans 104*, 29697–29713.

White W.M., Albarède F. & Télouk P. 2000. High-precision analysis of Pb isotope ratios by multi-collector ICP-MS. *Chemical Geology 167*, 257–270.

Winter B.L., Johnson C.M. & Clark D.L. 1997. Strontium, neodymium, and lead isotope variations of authigenic and silicate sediment components from the Late Cenozoic Arctic Ocean: implications for sediment provenance and the source of trace metals in seawater. *Geochimica et Cosmochimica Acta 61*, 4181–4200.